Gas plume species identification by regression analyses

David Pogorzala, David Messinger, Carl Salvaggio, John Schott

Digital Imaging and Remote Sensing Laboratory
Chester F. Carlson Center for Imaging Science
Rochester Institute of Technology

ABSTRACT

Identification of constituent gases in effluent plumes is performed using linear least-squares regression techniques. Overhead thermal hyperspectral imagery is used for this study. Synthetic imagery is employed as the test-case for algorithm development. Synthetic images are generated by the Digital Imaging and Remote Sensing Image Generation (DIRSIG) Model. The use of synthetic data provides a direct measure of the success of the algorithm through the comparison with truth map outputs. In image test-cases, plumes emanating from factory stacks will have been identified using a separate detection algorithm. The gas identification algorithm being developed in this work will then be used only on pixels having been determined to contain the plume. Stepwise linear regression is considered in this study. Stepwise regression is attractive for this application as only those gases truly in the plume will be present in the final model. Preliminary results from the study show that stepwise regression is successful at correctly identifying the gases present in a plume. Analysis of the results indicates that the spectral overlap of absorption features in different gas species leads to false identifications.

Keywords: gaseous plumes, hyperspectral, stepwise regression, target identification

1. INTRODUCTION

Prompted by growing concerns in environmental monitoring and national security, the detection and identification of gaseous plumes using hyperspectral imagery has become the topic of several recent studies.[1–4] Many of these investigations use image processing techniques commonly applied in the visible (VIS) and near infrared (NIR) portion of the electromagnetic spectrum on longwave infrared (LWIR) imagery. While many of these studies were successful in their ability to detect plume pixels in a scene, all of the techniques employed required prior knowledge of which gases were present in the scene.

Marinelli, *et al.* (2000)[1] identified dimethyl methylphosphonate (DMMP) and SF_6 being released from a small stack on the ground in front of a warm building. They show that a Spectral Matched Filter will detect the plume in the scene. However, the process requires the user to define the wavelengths of interest based on features of the gas in question. Lisowski and Cook (1996)[2] use normalized band differencing to detect SO_2 in overhead imagery. Again, a user is required since the background is normalized to the absorption peak of SO_2 before subtraction. Harig, *et al.* (2002)[3] compute a correlation coefficient between an atmosphere-subtracted pixel spectrum and the library absorption spectrum of a gas in specified spectral windows. This notion of using a subset of spectral windows for each material (*i.e.,* gas species) was established by Clark, *et al.* (1990).[5] This is an attractive possibility for the gas problem since absorption features of gases are pronounced and often distinct from one gas to another. Young (2002)[4] performed gas detection using a spectral matched filter and gas identification using both constrained and unconstrained linear regression. The basis vector set in his regression model is restricted to five gases, all at a single temperature. These gases were known to be the effluents from a refining plant in the scene. Young (2002) is successful at differentiating between plumes containing different gases using this method.

The work done here attempts to use linear regression techniques to identify the gases in *pre-detected* plumes in a hyperspectral image. The resulting algorithm is meant to run without user interaction and no prior knowledge of which gases are likely to be present in the scene. Standard matrix regression is not implemented since it forces a solution for each basis vector in the model regardless of whether or not that gas is present in the plume.

Further information: Chester F. Carlson Center for Imaging Science, Rochester Institute of Technolgy, 54 Lomb Memorial Dr., Rochester, NY 14623, drp9420@cis.rit.edu

Algorithms and Technologies for Multispectral, Hyperspectral, and Ultraspectral Imagery X, edited by Sylvia S. Shen, Paul E. Lewis, Proceedings of SPIE Vol. 5425 (SPIE, Bellingham, WA, 2004) · 0277-786X/04/$15 · doi: 10.1117/12.541641

Rather, stepwise regression, an iterative approach that eliminates needless basis vectors from the model, is used. Stepwise regression has been shown to be successful at selecting the appropriate basis vectors (endmembers) in unmixing hyperspectral VIS/NIR pixels.[6] No constraints are placed on the regression in this study.

This paper is organized in the following way. Synthetic image data, stepwise regression and the radiance model used to describe the plume are described in Section 2. Results from applying the identification algorithm to the synthetic imagery are discussed in Section 3. Section 4 includes a summary of the investigation as well as an outline of future work.

2. METHODOLOGY

2.1. Data

Synthetically generated imagery is the source of data for this study. Data generated by the Digital Imaging and Remote Sensing Image Generation (DIRSIG) model is attractive since the user has control over the types and quantities of gases being released by plumes in the scene. This allows for images to be generated that are inherently "ground-truthed". The user populates the scene with objects generated in CAD design software, and attributes these objects with field-measured properties such as spectral reflectance, thermal conductivity and spectral emissivity. Atmospheric effects are modeled with MODTRAN. For more information see Schott, *et al.* (1999).[7]

The plume model within DIRSIG is the Jet Propulsion Laboratory (JPL) Plume Model.[8] Spatially, the plume is constructed by modifying the gas concentration. In the downwind direction the concentration follows an exponential decay. In the across-track direction the concentration follows a Gaussian distribution. The width of the Gaussian increases as the plume travels further downwind. The result represents a time average of a plume rather than an instantaneous snapshot of a dynamic plume of gas. The JPL model gives depth to the plume by defining it as a cloud of points, each carrying with it the temperature and concentration of the gas at that location. When DIRSIG traces a ray from the sensor down through the plume, it encounters these points and integrates the radiative transfer along the path of the ray. This approach can reproduce phenomenology that a single slab model can not.

The DIRSIG model was used to create two scenes. The first contains no plumes and serves as the "background" in the radiance model described in Section 2.4. The second is simply a copy of the first scene, modified with two factory stacks releasing two separate plumes. One plume contains NH_3 gas and the other freon-114. The stacks were placed such that the two plumes do not overlap at any point downwind. The images measure 256 lines by 256 samples by $J = 128$ bands, from $7.5\mu m$ to $13.6\mu m$. The number of bands, as well as the band centers, were chosen to model the SEBASS (Spectrally Enhanced Broadband Array Spectrometer System) sensor. A single band at $10.73\mu m$ from the plume image is shown in Figure 1. The two plumes are clearly seen moving from the middle of the scene to the upper-right corner.

The gas absorption spectra used to generate the scene are supplied by the Pacific Northwest National Laboratory (PNNL) Spectral Library.[9] These spectra are measured at three temperatures, 5, 25 and 50° C. Both plumes in the scene use the 50° spectra. Thirty-one gases from this library are also used as the basis vector set in the stepwise regression discussed in Section 2.3.

2.2. Matrix Regression

Unmixing a hyperspectral pixel into its component endmembers (basis vectors) can be treated as a matrix regression. The standard model for regression in matrix form is[10]

$$\mathbf{x} = \mathbf{A}\mathbf{f} + \boldsymbol{\epsilon}, \tag{1}$$

where $\mathbf{x}$ is a $(J \times 1)$ pixel vector, $\mathbf{A}$ is a $(J \times N)$ matrix of N basis vectors, $\mathbf{f}$ is a $(N \times 1)$ vector of basis vector abundances, and $\boldsymbol{\epsilon}$ is a $(J \times 1)$ error term. The abundance coefficients, $\mathbf{f}$, are solved for as

$$\mathbf{f} = \mathbf{A}^{\dagger}\,\mathbf{x},$$

where $\mathbf{A}^{\dagger}$ denotes the pseudo-inverse of $\mathbf{A}$ and is defined as $\mathbf{A}^{\dagger} = (\mathbf{A}'\mathbf{A})^{-1}\,\mathbf{A}'$.

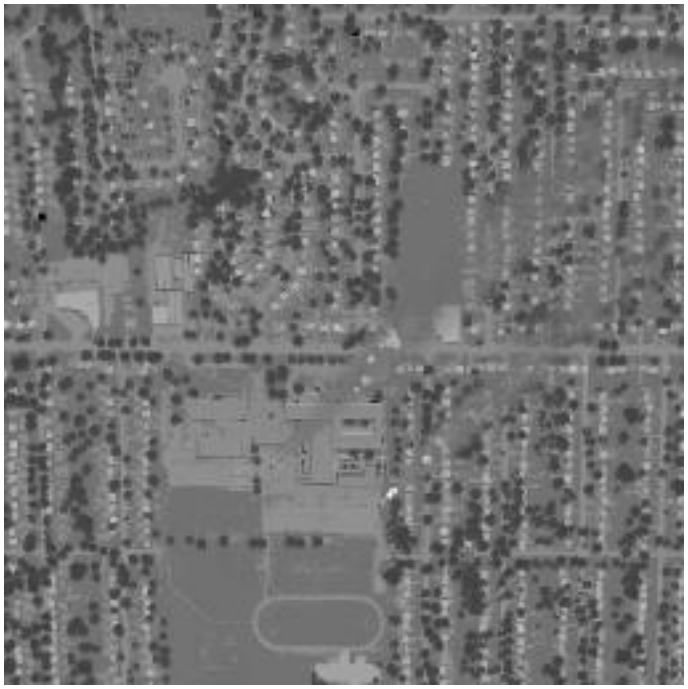

Figure 1. Single-band image of synthetic DIRSIG data at $10.73\mu m$. Both plumes can be seen moving from the middle of the scene to the upper-right corner. The NH_3 plume is the left-most plume while the freon-114 plume is on the right.

2.3. Stepwise Linear Regression

Stepwise regression begins by populating the matrix $\mathbf{A}$ with each of the M candidate basis vectors in turn. An F-test is used to determine which candidate vector best fits the data. The $M-1$ remaining vectors are then added to $\mathbf{A}$ in a similar fashion. The significance of adding a second vector to the regression model is determined using the Analysis of Variance (ANOVA) technique described below.[6] Once the model contains $N=2$ vectors, the $M-2$ remaining vectors are tested and, if necessary, one is added. After a third vector is added, each of the $N=3$ vectors in the model are removed in turn to ensure that each are contributing to the fit of the model. Candidate vectors are added and subtracted in this fashion until the fit of the model to the pixel spectrum can not be improved.

The ANOVA technique mentioned above calculates how much of the total variation about the mean (Sum of Squares (SS)), $\mathbf{x}'\mathbf{x}$, is due to the regression model (SSR), $\mathbf{f}'\mathbf{A}'\mathbf{x}$, and how much is from random errors (SSE), $\mathbf{x}'\mathbf{x}-\mathbf{f}'\mathbf{A}'\mathbf{x}$.[10] The ANOVA structure is depicted in Table 1. The Mean Squared (MS) column is defined by dividing the SS by the corresponding degrees of freedom (dof). In stepwise regression, ANOVA is useful in breaking the SSR of the N-element model down into the SSR due to the previous $(N-1)$-element model and the SSR due to the addition of the new term. If we define the $(N-1)$-element model as

$$\mathbf{x} = \mathbf{A}_{N-1}\mathbf{f}_{N-1} + \boldsymbol{\epsilon}, \tag{2}$$

then we can see how this fits into the ANOVA analysis in Table 1.

The MS terms from Table 1 can be used to create a statistic to test the quality of the regression model. This statistic is based upon the distribution of the error term, $\boldsymbol{\epsilon}$. It has been shown that if the model errors are independent and distributed as $\epsilon \sim N(0,\sigma^2)$, then the sum of the squares of these errors will be Chi-squared distributed with J dof abbreviated as χ^2_J.[10] Thus, we conclude that if the model is a good fit, then the sum-squared errors are Chi-squared distributed. If the model is a poor fit, then the errors will not follow this distribution. We formulate this as a hypothesis test, defining a null hypothesis that the abundance coefficient

Table 1. Sum of Squares ANOVA Table

Source	dof	SS	MS
Total SS	J	$\mathbf{x}'\mathbf{x}$	
SS Due to Regression (SSR)	N	$\mathbf{f}'\mathbf{A}'\mathbf{x}$	
SS About Regression (SSE) (residuals)	$J-N$	$\mathbf{x}'\mathbf{x}-\mathbf{f}'\mathbf{A}'\mathbf{x}$	$MSE=s^2$
SSR Reduced Model	$N-1$	$\mathbf{f}'_{N-1}\mathbf{A}'_{N-1}\mathbf{x}$	
SSR Extra Term	1	$\mathbf{f}'\mathbf{A}'\mathbf{x}-\mathbf{f}'_{N-1}\mathbf{A}'_{N-1}\mathbf{x}$	MS_{extra}

for the i^{th} basis vector, $\mathbf{f}_i$, is zero. The corresponding alternate hypothesis is that the coefficient is non-zero,

$$\begin{aligned} H_0: &\quad \mathbf{f}_i = 0 \\ H_1: &\quad \mathbf{f}_i \neq 0. \end{aligned}$$

As long as the null hypothesis is true, then the ratio of the mean-squared errors,

$$\frac{MS_{extra}}{MSE} \tag{3}$$

follows an $F_{1,J-N}$ distribution.[6] For this work the F-statistic was calculated at a probability of 0.99. When attempting to add a basis vector to the model, the ratio in Equation (3) is computed. If the ratio is smaller than the F-statistic then the null hypothesis is true and the vector is rejected. If the ratio is larger than the threshold, then it is added to the model. The algorithm terminates when no vectors are either added to or subtracted from the model.

2.4. Radiance Model

The radiance equation used to model the plume problem is derived here. We start with a standard model for a mixed pixel in the LWIR spectral region, where the pixel radiance, $L(\lambda)$, is a linear combination of C background materials. This "background pixel" is expressed as,

$$L_s(\lambda) = \left(\sum_{j=1}^{C} \beta_j \, \epsilon_j(\lambda) \, B(\lambda, T_s) \right) \tau_{atm}(\lambda) \; + \; L_u(\lambda), \tag{4}$$

where β_j is the mixing coefficient for the j^{th} background material, $\epsilon_j(\lambda)$ is the spectral emissivity of the j^{th} background material, $B(\lambda, T_s)$ is the Planck radiance function evaluated at the surface temperature, T_s, τ_{atm} is the atmospheric transmission and L_u is the upwelled radiance. Reflected downwelled radiance has been excluded from Equation (4) due to the fact that many materials have a high, uniform emissivity in the LWIR.[11] This translates into a low, uniform reflectivity that does not have a significant impact on the sensor-reaching radiance.

When writing an expression for the radiance of a pixel containing a plume (*i.e.,* a "target" pixel) we can make several approximations. We assume that the plume's self-radiation does not significantly reflect off of the ground and back up to the sensor. We neglect any scattering by the plume and any entrainment of ambient air within the plume. We also assume that all of the individual gases within the plume are at the same temperature. These assumptions allow us to write the sensor-reaching radiance for a plume pixel as

$$L_p(\lambda) = \left(\left[\sum_{j=1}^{C} \beta_j \, \epsilon_j(\lambda) \, B(\lambda, T_s) \right] \tau_p(\lambda) \; + \; \epsilon_p(\lambda) \, B(\lambda, T_p) \right) \tau_{atm}(\lambda) \; + \; L_u(\lambda), \tag{5}$$

where the subscript p denotes quantities related to the plume. Equation (5) shows that the self-emitted radiance from the background is attenuated by the plume. Both this radiance and the self-emitted radiance from the plume are then attenuated by the atmosphere.

Recalling Kirchoff's Law, we can equate the absorption of a gas to its emission as

$$\epsilon_p(\lambda) = \sum_{i=1}^{D} c_i \, k_i(\lambda) \tag{6}$$

where c_i is the column density and k_i is the absorption spectrum of gas i. In addition, conservation of energy says that if the gas is optically thin, we can set $\tau = 1 - \epsilon$. Substituting these changes into Equation (5) results in the final model for a pixel containing multiple background materials and multiple gases as

$$L(\lambda) = \left(\left[\sum_{j=1}^{C} \beta_j \, \epsilon_j(\lambda) \, B(\lambda, T_s) \right] \left[1 - \sum_{i=1}^{D} c_i \, k_i(\lambda) \right] \; + \; \left[\sum_{i=1}^{D} c_i \, k_i(\lambda) \right] B(\lambda, T_p) \right) \tau_{atm}(\lambda) \; + \; L_u(\lambda). \tag{7}$$

From this point on, we will drop the atmospheric terms from the radiance model. This does not indicate that atmospheric compensation has been done to the data. The benefit of atmospheric compensation to the identification algorithm will be investigated in a future study.

The background term in Equation (7) contains $2C+1$ unknown terms; C background ratios, β_j, C background emissivities, $\epsilon_j(\lambda)$, and the background temperature, T_s. The need to solve for these is eliminated by the use of the plume-free synthetic image discussed in Section 2.1. On a pixel-by-pixel basis, the background under the plume is expressed as $L_{(x,y)}(\lambda)$, where (x, y) indicates the image coordinates of the pixel in question. The use of the exact background on a per-pixel basis is admittedly over-simplistic. It is used here only as the first step in the algorithm development process. A rigorous characterization of the background will be the focus of further studies. Substituting this in for the background term, and distributing that through the plume transmission term, we arrive at,

$$L(\lambda) = L_{(x,y)}(\lambda) - L_{(x,y)}(\lambda) \sum_{i=1}^{D} c_i \, k_i(\lambda) \; + \; \left[\sum_{i=1}^{D} c_i \, k_i(\lambda) \right] B(\lambda, T_p). \tag{8}$$

We can now subtract the first background term from both sides and factor out the plume emissivity term to arrive at,

$$L(\lambda) - L_{(x,y)}(\lambda) = \sum_{i=1}^{D} c_i k_i(\lambda) \left[B(\lambda, T_p) - L_{(x,y)}(\lambda) \right]. \tag{9}$$

The only unsolved parameter in Equation (9) is the plume temperature, T_p. While it is not necessary to solve for this value explicitly, we must address it to some degree. Specifically, we must take into account the temperature difference between the plume and the surface. Assuming a relatively flat surface emissivity spectrum, the plume is seen in emission if this *temperature contrast* is positive. If the surface is warmer than the plume and the contrast is negative, then the plume is in absorption. The difference between emission and absorption is critical as it dictates the direction of the gas features (peaks or troughs) in the pixel. Since we are attempting to identify the gases by fitting a set of basis vectors to the pixel spectrum, we need to ensure that the basis vector set accounts for both emission and absorption. We do so by defining a temperature contrast term, ΔT, and replacing T_p by $(T_s \pm \Delta T)$. The surface temperature, T_s, while not known, is estimated on a pixel-by-pixel basis by inverting $L_{(x,y)}(\lambda)$ to solve for the spectral brightness temperature, $T_{s,(x,y)}(\lambda)$. The maximum of $T_{s,(x,y)}(\lambda)$ is selected as the surface temperature *estimate*, $\widehat{T}_{s,(x,y)}$. Replacing this for T_p in Equation (9) brings us to the final equation for a plume pixel,

$$L(\lambda) - L_{(x,y)}(\lambda) = \sum_{i=1}^{D} c_i k_i(\lambda) \left[B(\lambda, \, \widehat{T}_{s,(x,y)} \pm \Delta T) - L_{(x,y)}(\lambda) \right]. \tag{10}$$

By defining various positive and negative values for ΔT, we can easily account for both the emission and absorption of the plume gases. In addition, this form now resembles the standard equation for matrix regression

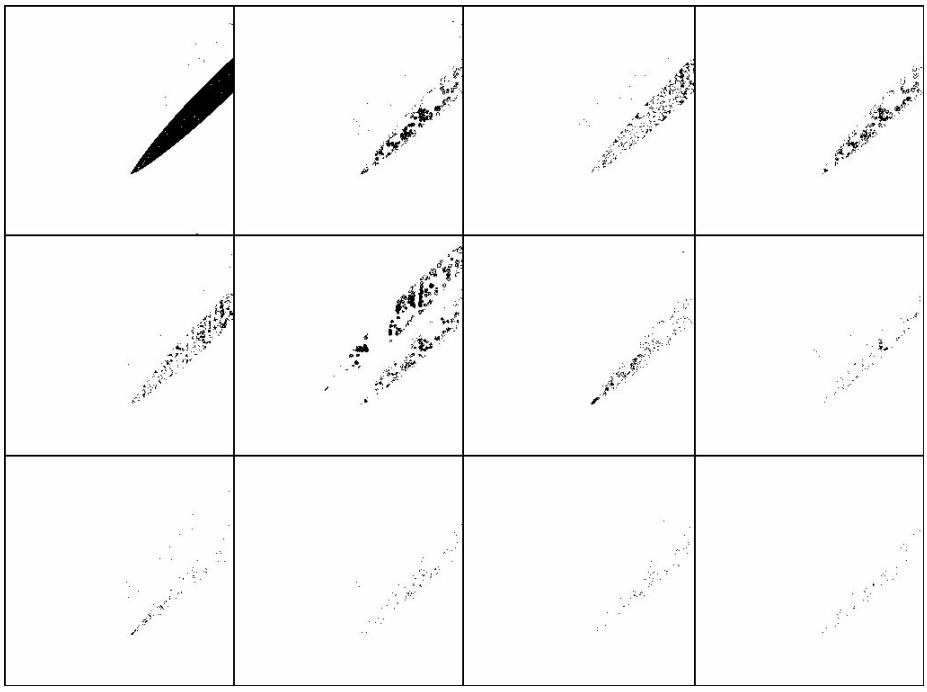

Figure 2. Detection maps of the freon-114 plume from the application of stepwise regression to the image. The upper-left image is the map for freon-114 gas (correct identification). Moving across each row are the "top 11" false alarms; phg, tce, edb, SO_2, hyd, vcl, C_6H_6, HCHO, dclp-13, CO, and CH_4. The maps have been inverted such that black indicates a positive identification.

in Equation (1), where the abundance fractions to be solved for, $\mathbf{f}$, are the relative gas concentration path-lengths, c_i, and the matrix of basis vectors, $\mathbf{A}$, is the absorption spectrum multiplied by the plume-background radiance contrast, $k_i(\lambda)\left[B(\lambda, \widehat{T}_{s,(x,y)} \pm \Delta T) - L_{(x,y)}(\lambda)\right]$.

3. RESULTS

The algorithm was applied to only those pixels known to contain plume gases. A by-product of the synthetic image is a "truth map" that indicates the spatial location of the plume. This was used to mask out non-plume pixels. In applying the algorithm to real imagery, it is assumed that the plumes have been detected by a separate process. The raw output from the algorithm is M binary maps ($M = 440$), one for each basis vector, indicating in which pixels that vector was found by the regression. This value for M is the result of multiplying 88 gas spectra from the PNNL library by 5 values of ΔT; -10, -5, 0, +5 and +10°C. These images were then collapsed to 31 maps, one per gas species, showing every pixel in which any basis vector representing gas i was found.

Figure 2 shows the collapsed output map for freon-114 gas, along with the "top 11" false alarm gases. These false alarms were chosen by visual inspection of the 31 gas maps. They are arranged in order from most to fewest false alarms. A listing of the gases, along with their false alarm rank and abbreviation is found in Table 2. Gases not included in Figure 2 had very few false alarms in the freon-114 plume and are not considered in the analysis.

The algorithm was successful in correctly identifying freon-114. However, the ability to detect the gas in nearly every plume pixel is unrealistic. This is attributed to the lack of sensor noise in the synthetic image, and the fact that the exact background was used on a per-pixel basis. Despite these advantages, the algorithm wrongly identified several gases. The reason for this is believed to be the overlap of several key absorption features in freon-114 and the worst of the false alarm candidates. This is depicted in Figure 3, which shows the normalized absorption spectrum of freon-114 along with the spectra of the "top 11" false alarm-producing library

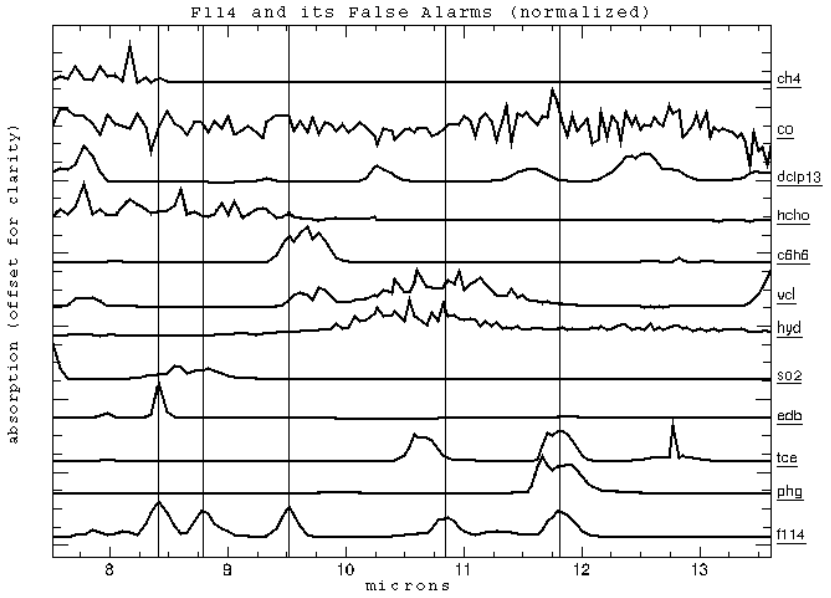

Figure 3. Absorption spectrum for freon-114 along with the spectra of the "top 11" false alarms. Each spectrum has been normalized to its own maximum.

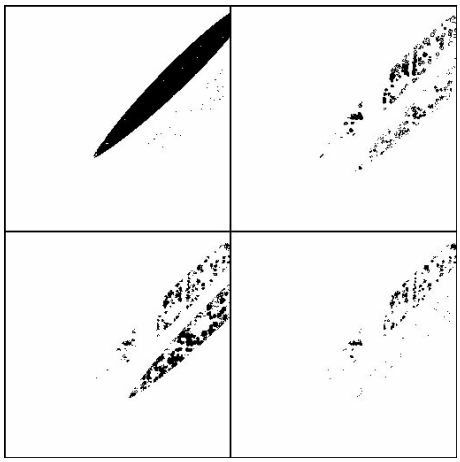

Figure 4. Detection maps of the ammonia (NH_3) plume from the application of stepwise regression to the image. The upper-left image is the map for NH_3 gas (correct identification). Moving across each row are the "top 3" false alarms; hyd, freon-12 and acrolein. The maps have been inverted such that black indicates a positive identification.

gases (offset for clarity). The spectra of phosgene and trichloroethylene both contain a significant absorption feature at approximately $11.8\mu m$. These features clearly overlap with the feature on freon-114. Dibromoethane is also seen as having an overlapping feature at approximately $8.4\mu m$. This spectral overlap causes the regression to wrongly fit these gases to the background-subtracted pixel spectrum.

Figure 4 shows the collapsed output map for NH_3 gas, along with the "top 3" false alarm gases. The false alarms are arranged here in the same manner as the freon-114 plume above. Again, the detection of NH_3 is unrealistic for the same reasons. The normalized absorption spectra of all four gases are shown in Figure 5. The spectral overlap is not as obvious here as in Figure 3. This is because the absorption features in NH_3 are narrower than they are for freon-114. However significant overlap is evident. Hydrazine is seen as having

Table 2. Table of gas name abbreviations.

Plume	Gas name	Symbol	False Alarm Rank
Freon-114			
	Freon-114	f114	-
	Phosgene	phg	1
	Trichloroethylene	tce	2
	Dibromoethane	edb	3
	Sulfur Dioxide	SO_2	4
	Hydrazine	hyd	5
	Vinyl Chloride	vcl	6
	Benzene	C_6H_6	7
	Formaldehyde	HCHO	8
	Dichloropropane	dclp-13	9
	Carbon Monoxide	CO	10
	Methane	CH_4	11
NH_3			
	Ammonia	NH_3	-
	Hydrazine	hyd	1
	Freon-12	f12	2
	Acrolein	acrol	3

overlapping features at approximately 9.9, 10.1, 10.4 and 10.75μm, freon-12 at approximately 9.1 and 10.75μm, and acrolein at approximately 9.9, 10.1 and 10.4μm. Again this supports the theory that spectral overlap will cause the regression to wrongly fit these gases to the background-subtracted pixel spectrum.

4. CONCLUSIONS

Unconstrained stepwise linear regression was used to identify the gases present in pixels pre-defined as containing a gas plume. Synthetic imagery was used containing a freon-114 plume and an NH_3 plume. Absorption spectra of 31 gases were multiplied by 5 temperature contrast values to generate the library of potential basis vectors. A series of output maps were generated for each basis vector and subsequently collapsed to a per-species level. The output maps for freon-114 and NH_3 were visually compared to those of gases falsely identified. Spectral overlap has been identified as the primary source of false gas identifications.

Further work in this study will investigate three topics. The first will attempt to negate the effects of spectral overlap. Options such as performing the stepwise regression in selective spectral windows will be investigated. The second topic will be to replace the use of the exact background on a per-pixel basis with a background approximation. A linear combination of background endmembers and a clustering of non-plume pixels in the vicinity of the plume will be considered. The third task to investigate is the application of the identification algorithm to atmospherically compensated data.

ACKNOWLEDGMENTS

This work was funded under the Office of Naval Research Multi-disciplinary University Research Initiative "Model-based Hyperspectral Exploitation Algorithm Development" #N00014-01-1-0867

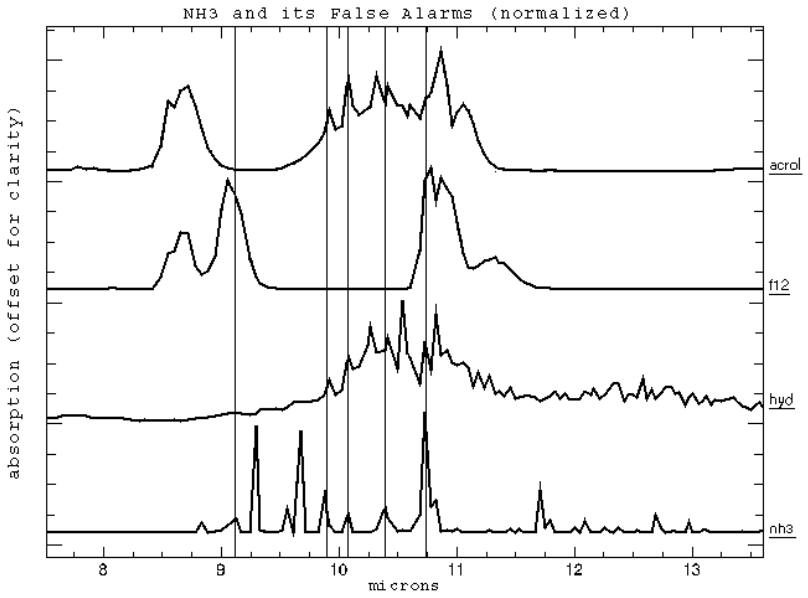

Figure 5. Absorption spectrum for NH_3 along with the spectra of the "top 3" false alarms. Each spectrum has been normalized to its own maximum.

REFERENCES

1. W. Marinelli, C. Gittins, A. Gelb, and B. Green, "A tunable fabry-perot etalon-based long-wavelength infrared imaging specroradiometer," *Applied Optics* **38**(12), pp. 2594–2604, 2000.
2. J. Lisowski and C. Cook, "A svd method for spectral decomposition and classification of ares data," in *SPIE Optical Science, Engineering and Instrumentation Annual Meeting*, *Proc. of SPIE* **2821**, pp. 14–29, 1996.
3. R. Harig, G. Matz, and P. Rusch, "Scanning infrared remote sensing system for identification, visualization and quantification of airborne pollutants," in *Instrumentation for Air Pollution and Global Atmospheric Monitoring*, J. Jensen and R. Spellicy, eds., *Proc. of SPIE* **4574**, pp. 83–94, 2002.
4. S. Young, "Detection and quantification of gases in industrial-stack plumes using thermal-infrared hyperspectral imaging," Tech. Rep. Report No. ATR-2002(8407)-1, The Aerospace Corporation, 2002.
5. R. Clark, A. Gallagher, and G. Swayze, "Material absorption band depth mapping of imaging spectrometer data using a complete band shape least-squares fit with library reference spectra," *Proceedings of the Second Airborne Visible/Infrared Imaging Spectrometer (AVIRIS) Workshop* , pp. 176–186, 1990a.
6. H. Gross and J. Schott, "Application of spatial resolution enhacement and spectral mixture analysis to hyperspectral images," *SPIE Optical Science, Engineering, and Instrumentation Annual Meeting* **2821**, pp. 30–41, 1996.
7. J. Schott, S. Brown, R. Raqueño, H. Gross, and G. Robinson, "An advanced synthetic image generation model and its application to multi/hyperspectral algorithm development," *Canadian Journal of Remote Sensing* **25**(2), pp. 99–111, 1999.
8. S. Kuo, J. Schott, and C. Chang, "Synthetic image generation of chemical plumes for hyperspectral applications," *Optical Engineering* **39**(4), pp. 1047–1056, 2000.
9. S. Sharp *et al.*, "Creation of 0.10 cm^{-1} resolution, quantitative, infrared spectral libraries for gas samples," in *Vibrational Spectroscopy-Based Sensor Systems*, S. Christesen and I. A.J. Sedlacek, eds., *Proc. of SPIE* **4577**, pp. 12–24, 2001.
10. N. Draper and H. Smith, *Applied Regression Analysis, 2^{nd} ed.*, John Wiley & Sons, New York, 1981.
11. D. Gu, A. Gillespie, A. Kahle, and F. Palluconi, "Autonomous atmospheric compensation (aac) of high resolution hyperspectral thermal infrared remote-sensing imagery," *IEEE Transactions on Geoscience and Remote Sensing* **38**(6), pp. 2557–2570, 2000.